Journal of Solid State Chemistry **145,** 174–181 (1999)
Article ID jssc.1999.8236, available online at http://www.idealibrary.com on IDEAL®

Syntheses, Crystal Structures, and Properties of EuRhIn, $EuIr_2$, and $EuIrSn_2$

Rainer Pöttgen,*,[1] Rolf-Dieter Hoffmann,* Manfred H. Möller,* Gunter Kotzyba,* Bernd Künnen,* Carsten Rosenhahn,† and Bernd D. Mosel†,[1]

*Anorganisch-Chemisches Institut, Universität Münster, Wilhelm-Klemm-Straße 8, D-48149 Münster, Germany; and
†Institut für Physikalische Chemie, Universität Münster, Schloßplatz 4/7, D-48149 Münster, Germany

Received October 5, 1998; in revised form February 19, 1999; accepted February 23, 1999

The title compounds were prepared from the elements by reactions in sealed tantalum tubes in a high-frequency furnace. Their structures were refined from single crystal X-ray diffractometer data: *Pnma*, $a = 744.4(1)$ pm, $b = 434.15(9)$ pm, $c = 845.5(1)$ pm, $wR2 = 0.0433$, 658 F^2 values, 20 variables for EuRhIn, *Fd3m*, $a = 756.5(1)$ pm, $wR2 = 0.0349$, 94 F^2 values, 5 variables for $EuIr_2$, and *Cmcm*, $a = 434.78(3)$ pm, $b = 1124.0(1)$ pm, $c = 751.20(5)$ pm, $wR2 = 0.0561$, 565 F^2 values, 16 variables for $EuIrSn_2$. EuRhIn crystallizes with a TiNiSi type structure that consists of strongly puckered Rh_3In_3 hexagons. The europium atoms fill the channels within the three-dimensional [RhIn] polyanion. EuRhIn orders ferromagnetically at 22.0(5) K with a saturation magnetic moment of 6.7(1) μ_B/Eu at 4 K and 5.5 T. The divalent character of the europium atoms in EuRhIn was determined from temperature dependent susceptibility (7.9 μ_B/Eu in the high-temperature part) and ^{151}Eu Mössbauer spectroscopic experiments. The latter show an isomer shift of $\delta = -8.30(2)$ mm/s at 78 K. At 4.2 K full magnetic hyperfine field splitting subjected to significant quadrupole splitting of $\Delta E_Q = 8$ mm/s is observed. EuRhIn is a metallic conductor with a room temperature value of 58 μΩcm for the specific resistivity. The structure of the Laves phase $EuIr_2$ is confirmed on the basis of single crystal X-ray data. The iridium atoms form a tetrahedral network with Ir–Ir distances of 268 pm. $EuIrSn_2$ adopts a $MgCuAl_2$ type structure that may be described as an iridium-filled variant of a distorted $CaIn_2$-like sublattice of composition $EuSn_2$. The tin atoms in the distorted and puckered hexagonal network have shorter (303 and 322 pm) and longer (343 pm) tin-tin contacts. © 1999 Academic press

Key Words: **intermetallic europium compounds; crystal structure; magnetism; ^{151}Eu Mössbauer spectroscopy.**

INTRODUCTION

The equiatomic intermetallic europium compounds $EuTX$ (T = transition metal, X = main group element) have intensively been investigated in recent years with respect to their crystal structures and physical properties (1–8, and ref. therein). Some remarkable compounds within this family are the mixed-valent pnictides EuPtP and EuPdAs (3, 7), the stannide EuAuSn (6) with a complex superstructure of the KHg_2 type, and the metamagnets EuPdIn, EuPtIn, and EuAuIn (8). Although a huge number of equiatomic europium compounds have been reported, the only compounds with rhodium and iridium as transition metal component are EuRhGa (9) and EuIrP (10). We have recently started a more systematic study on the structure–property relationships of these equiatomic intermetallic europium compounds, especially on the germanides, stannides, and indium compounds (4, 6, 8, and ref. therein). During these investigations we synthesized the new ferromagnet EuRhIn, presented in the present paper. When searching for the possible equiatomic compounds "EuIrIn" and "EuIrSn" we obtained high quality single crystals of the Laves phase $EuIr_2$ and the new stannide $EuIrSn_2$. Both structure refinements are reported herein. Binary $EuIr_2$ has previously been reported only from X-ray powder data (11).

EXPERIMENTAL

Starting materials for the preparation of EuRhIn, $EuIr_2$, and $EuIrSn_2$ were ingots of europium (Johnson Matthey), rhodium powder (Degussa, 200 mesh), iridium powder (Degussa, 200 mesh), indium tear drops (Johnson-Matthey), and tin granules (Merck), all with stated purities greater than 99.9%. The large europium ingots were cut into small pieces in a glove box. They were not allowed to contact air prior to the reactions. The elemental components were mixed in the ideal atomic ratios and sealed in tantalum tubes under an argon pressure of about 800 mbar. The argon was purified over molecular sieves, titanium sponge (900 K), and an oxisorb catalyst (12). The tantalum tubes were subsequently sealed in silica ampoules to prevent oxidation and at first heated at 1220 K for two days. The

[1]To whom correspondence should be addressed. E-mail: pottgen@uni-muenster.de and mosel@uni-muenster.de.

0022-4596/99 $30.00

temperature was subsequently lowered by 50 K/day and held at 970 K for a further 3 weeks. The reactions resulted in polycrystalline products that could readily be separated from the tantalum tubes. Alternatively, the tantalum tubes can directly be heated in a water-cooled sample chamber in a high-frequency furnace as described in detail in reference 13.

Although $EuIr_2$ and EuRhIn were obtained as single phase samples, this was not possible for $EuIrSn_2$. This stannide was obtained in a yield of about 90% from a sample of the starting composition Eu:Ir:Sn = 1:1:1. With an initial composition Eu:Ir:Sn = 1:1:2 we obtained a new tin-rich stannide of the approximate composition $\sim EuIrSn_3$ (14). The compositions were obtained from EDX analyses of polished samples of the initial 1:1:2 composition. The 1:1:1 samples contained a small amout of binary $EuIr_2$ as a parasitic phase. A similar observation was also recently made in the ternary system calcium–iridium–indium (14). We attribute this to the high melting point (2680 K) of iridium, which is much higher than those of europium (1100 K) and tin (505 K). This most likely avoids a complete reaction of the initial reaction components. Since the $EuIrSn_2$ samples always contained small amounts of a parasitic phase, the measurement of the physical properties of this stannide was not possible.

Powders and single crystals of the investigated europium compounds show a light gray color and are stable in air. No decomposition whatsoever was observed after several months. The irregularly shaped single crystals exhibit silvery metallic luster.

Guinier powder patterns of the samples were recorded at room temperature with Cu$K\alpha_1$ radiation using α-quartz ($a = 491.30$ pm, $c = 540.46$ pm) as an internal standard. The lattice constants (see Table 1) were obtained from least-squares fits of the Guinier data. To assure correct indexing, the observed patterns were compared with calculated ones (15) taking the atomic positions from the structure refinements. In all cases the lattice constants determined from the powders and those from single crystals agreed well.

Single crystal intensity data were collected at room temperature by use of a four-circle diffractometer (CAD4) with graphite monochromatized Mo$K\alpha$ radiation (0.71073 pm) and a scintillation counter with pulse height discrimination. The scans were performed in the $\omega/2\theta$ mode. Empirical absorption corrections were applied on the basis of psi-scan data.

The magnetic susceptibilities of polycrystalline pieces of EuRhIn were determined with a SQUID magnetometer (Quantum Design, Inc.) between 2 and 300 K with magnetic flux densities up to 5.5 T. The specific resistivities were measured on small blocks with a conventional four-probe technique over the temperature range from 4.2 to 300 K. Cooling and heating curves were identical within the error limits and were reproducible for different samples.

The 21.53 keV transition of ^{151}Eu with an activity of 130 MBq (2% of the total activity of a ^{151}Sm:EuF_3 source) was used for the Mössbauer spectroscopic experiments. The measurements were performed with a commercial helium bath cryostat. The temperature of the absorber could be varied from 4.2 to 300 K and was measured with a metallic resistance thermometer with a precision better than ± 0.5 K. The source was kept at room temperature. The material for the Mössbauer spectroscopic measurements was the same as for the susceptibility and resistivity measurements. The sample was placed within a thin-walled PVC container at a thickness corresponding to about 10 mg Eu/cm^2.

RESULTS AND DISCUSSION

Structure Refinements

Irregularly shaped single crystals of EuRhIn, $EuIr_2$, and $EuIrSn_2$ were isolated from the annealed samples and were examined by use of a Buerger precession camera. The precession photographs (reciprocal layers *hk*0 and *h*0*l* for

TABLE 1
Lattice Constants of EuRhIn, $EuIr_2$, and $EuIrSn_2$

Compound	Structure type	Space group	*a* (pm)	*b* (pm)	*c* (pm)	*V* (nm^3)	Reference
EuRhIn	TiNiSi	*Pnma*	744.4(1)	434.15(9)	845.5(1)	0.2733(1)	This work
EuRhIn[a]	TiNiSi	*Pnma*	743.6(1)	433.7(1)	844.4(1)	0.2723(1)	This work
$EuIr_2$	$MgCu_2$	*Fd3m*	756.6	*a*	*a*	0.4331	11
$EuIr_2$	$MgCu_2$	*Fd3m*	756.5(1)	*a*	*a*	0.4329(1)	This work
$EuIr_2$[a]	$MgCu_2$	*Fd3m*	756.4(1)	*a*	*a*	0.4328(1)	This work
$EuIrSn_2$	$MgCuAl_2$	*Cmcm*	434.78(3)	1124.0(1)	751.20(5)	0.3671(1)	This work
$EuIrSn_2$[a]	$MgCuAl_2$	*Cmcm*	435.5(1)	1125.2(1)	751.8(1)	0.3684(1)	This work

Note. Standard deviations in the positions of the last significant digits are given in parentheses.
[a]These data were obtained on the four-circle diffractometer.

TABLE 2
Crystal Data and Structure Refinements for EuRhIn, $EuIr_2$, and $EuIrSn_2$

Empirical formula	EuRhIn	$EuIr_2$	$EuIrSn_2$
Molar mass (g/mol)	369.69	536.36	581.54
Space group, Z	*Pnma,* 4	*Fd3m,* 8	*Cmcm,* 4
Calculated density (g/cm^3)	8.99	16.46	10.52
Crystal size (μm^3)	$15 \times 25 \times 40$	$40 \times 40 \times 40$	$20 \times 40 \times 40$
Transmission ratio (max/min)	1.53	1.45	1.82
Absorption coefficient (mm^{-1})	36.6	150.8	66.2
$F(000)$	628	1736	960
θ range for data collection	2° to 35°	2° to 43°	2° to 38°
Range in hkl	± 11, $+6$, ± 13	± 14, ± 14, $+13$	± 7, ± 19, ± 12
Total no. of reflections	2481	1337	2216
Independent reflections	658 ($R_{int} = 0.0559$)	94 ($R_{int} = 0.1153$)	565 (R_{int} =0.0317)
Reflections with $I > 2\sigma(I)$	514 ($R_{sigma} = 0.0400$)	84 ($R_{sigma} = 0.0385$)	531 ($R_{sigma} = 0.0209$)
Data/restraints/parameters	658/0/20	94/0/5	565/0/16
Goodness-of-fit on F^2	1.040	1.069	1.178
Final R indices [$I > 2\sigma(I)$]	$R1 = 0.0200$	$R1 = 0.0149$	$R1 = 0.0233$
	$wR2 = 0.0384$	$wR2 = 0.0335$	$wR2 = 0.0549$
R indices (all data)	$R1 = 0.0394$	$R1 = 0.0165$	$R1 = 0.0258$
	$wR2 = 0.0433$	$wR2 = 0.0349$	$wR2 = 0.0561$
Extinction coefficient	0.0074(3)	0.0018(2)	0.0024(2)
Largest diff. peak and hole	2114 and -2417 e/nm^3	1821 and -2308 e/nm^3	4953 and -3695 e/nm^3

EuRhIn and $EuIrSn_2$ and $hk0$ for $EuIr_2$) were in good agreement with the unit cells listed in Table 1. The extinction conditions were compatible with the space groups *Pnma* (EuRhIn), *Fd3m* ($EuIr_2$), and *Cmcm* ($EuIrSn_2$). All relevant crystallographic data and experimental details for the data collections are listed in Table 2.

The starting atomic parameters were deduced from automatic interpretations of direct methods with SHELX-86 (16), and the structures were subsequently refined using SHELXL-97 (17) (full-matrix least-squares on F^2) with anisotropic atomic displacement parameters for all atoms. Final difference Fourier synthesis revealed no significant residual peaks (see Table 2). The highest peak for $EuIrSn_2$ was close to the iridium position (62 pm) and most likely resulted from an incomplete absorption correction. The positional parameters and interatomic distances of the refinements are listed in Tables 3 and 4. Listings of the anisotropic displacement parameters and structure factor tables are available.[2]

Magnetic and Electrical Properties of EuRhIn

The temperature dependence of the inverse magnetic susceptibility of EuRhIn measured at an external field strength of 3 T is presented in Fig. 1. Above 100 K EuRhIn shows Curie–Weiss behavior. The experimental magnetic moment determined from this high temperature part of the inverse susceptibility is 7.9(1) μ_B/Eu, in good agreement with the value of 7.94 μ_B for the free Eu^{2+} ion. The paramagnetic Curie temperature (Weiss constant) of 34(1) K was obtained by linear extrapolation of the high temperature part (data above 100 K) of the $1/\chi$ vs T plot to $1/\chi = 0$. The inset of Fig. 1 shows the low temperature behavior measured at 0.01 T. The almost vanishing inverse susceptibility and the

TABLE 3
Atomic Coordinates and Isotropic Displacement Parameters (pm^2) for EuRhIn, $EuIr_2$, and $EuIrSn_2$

Atom	Wyckoff site	x	y	z	U_{eq}
		EuRhIn (space group *Pnma*)			
Eu	4*c*	0.02690(5)	1/4	0.67586(4)	104(1)
Rh	4*c*	0.27739(8)	1/4	0.37308(6)	114(1)
In	4*c*	0.14525(6)	1/4	0.06385(6)	97(1)
		$EuIr_2$ (space group *Fd3m*)			
Eu	8*a*	1/8	1/8	1/8	74(2)
Ir	16*d*	1/2	1/2	1/2	61(1)
		$EuIrSn_2$ (space group *Cmcm*)			
Eu	4*c*	0	0.06467(4)	1/4	84(1)
Ir	4*c*	0	0.78737(3)	1/4	62(1)
Sn	8*f*	0	0.35077(4)	0.04857(6)	70(1)

Note. U_{eq} is defined as one-third of the trace of the orthogonalized U_{ij} tensor.

[2]Details may be obtained from Fachinformationszentrum Karlsruhe, D-76344 Eggenstein-Leopoldshafen (Germany), by quoting the Registry No's. CSD-410699 (EuRhIn), CSD-410701 ($EuIr_2$), and CSD-410700 ($EuIrSn_2$).

TABLE 4
Interatomic Distances (pm), Calculated with the Lattice Constants Taken from X-Ray Powder Data of EuRhIn, $EuIr_2$, and $EuIrSn_2$

EuRhIn				**$EuIr_2$**			
Eu:	2	Rh	310.1	Eu:	12	Ir	313.6
	2	Rh	316.5		4	Eu	327.6
	1	Rh	316.7				
	2	In	334.6	Ir:	6	Ir	267.5
	1	In	339.7		6	Eu	313.6
	2	In	340.1				
	1	In	349.0				
	2	Eu	370.4	**$EuIrSn_2$**			
	2	Eu	392.8	Eu:	1	Ir	311.7
	1	Rh	424.2		4	Sn	326.5
	2	Eu	434.2		2	Ir	331.5
					2	Sn	355.4
Rh:	2	In	276.5		4	Sn	357.7
	1	In	279.0		2	Eu	402.8
	1	In	279.4		2	Ir	410.8
	2	Eu	310.1		2	Eu	434.8
	2	Eu	316.5				
	1	Eu	316.7	Ir:	2	Sn	272.8
	1	Eu	424.2		4	Sn	274.3
					1	Eu	311.7
In:	2	Rh	276.5		2	Eu	331.5
	1	Rh	279.0		2	Eu	410.8
	1	Rh	279.4				
	2	In	324.9	Sn:	1	Ir	272.8
	2	Eu	334.6		2	Ir	274.3
	1	Eu	339.7		1	Sn	302.6
	2	Eu	340.1		2	Sn	322.3
	1	Eu	349.0		2	Eu	326.5
					1	Sn	343.3
					1	Eu	355.4
					2	Eu	355.7

Note. Standard deviations are all equal or less than 0.2 pm. All distances within the first coordination sphere are listed.

high positive Curie temperature indicate ferromagnetic ordering.

The precise Curie temperature of 22.0(5) K was determined from the derivative ($d\chi/dT$) of a *kink point* measurement in the field-cooling mode at a low flux density of 0.002 T (Fig. 2). The magnetization vs external field dependence at 4 K is shown in Fig. 3. The magnetization curve tends to saturate already at low flux densities. At the highest obtainable field of 5.5 T, the saturation magnetic moment is $\mu_{sm(exp)} = 6.7(1)\ \mu_B$/Eu, only slightly smaller than the theoretical value of $\mu_{sm(calc)} = 7.0\ \mu_B$/Eu, calculated from $\mu_{sm(calc)} = g \times J\ \mu_B$ (18). We have thus achieved an almost parallel spin alignment at 4 K and 5.5 T. Similar high saturation magnetizations have recently also been observed for EuCuAs, EuAgAs (1), EuPdIn (19, 20), EuPtIn (8), and EuZnSn (21). Because of the very narrow hysteresis, EuRhIn may be characterized as a very soft ferromagnet.

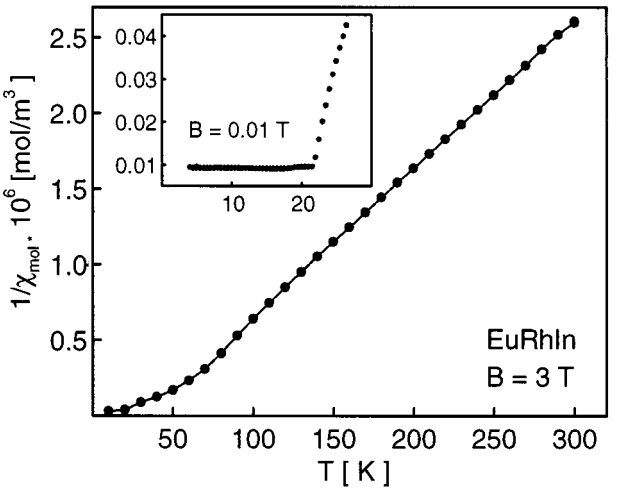

FIG. 1. Temperature dependence of the inverse magnetic susceptibility of EuRhIn measured at a magnetic flux density of 3 T. The inset shows the inverse susceptibility measured at 0.01 T at low temperatures.

The temperature dependence of the specific resistivity of EuRhIn is plotted in Fig. 4. The specific resistivity decreases with decreasing temperature, as is typical for metals. According to the room temperature value of 58 μΩcm, EuRhIn is a reasonably good conductor. At low temperature, the specific resistivity has dropped to 30 μΩcm. The steeper decrease below about 40 K is most likely due to the onset of magnetic ordering, resulting from freezing of spin-disorder scattering.

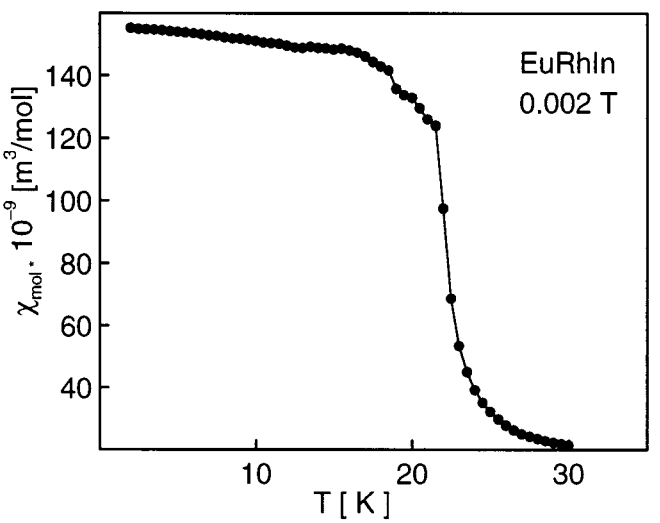

FIG. 2. Temperature dependence of the susceptibility of EuRhIn at low temperatures determined at a magnetic flux density of 0.002 T in the field-cooling mode.

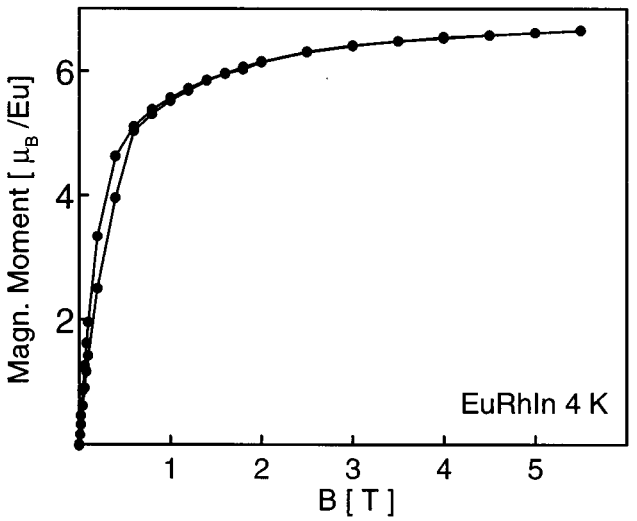

FIG. 3. Magnetization vs external field dependence of EuRhIn at 4 K.

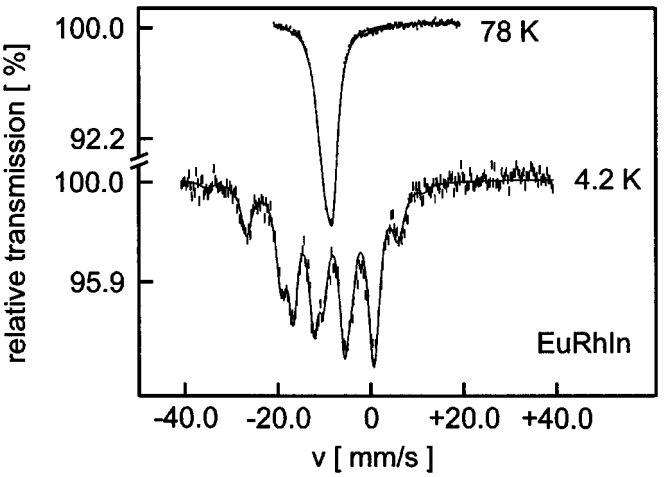

FIG. 5. Experimental and simulated ^{151}Eu Mössbauer spectra of EuRhIn at 4.2 and 78 K.

^{151}*Eu Mössbauer Spectroscopy of EuRhIn*

The ^{151}Eu Mössbauer spectra of EuRhIn at 4.2 and 78 K are shown in Fig. 5, together with transmission integral fits. The fitting parameters and the results of some additional temperatures are listed in Table 5. No Eu(III) impurity peak can be detected around $\delta = 0$ mm/s, indicating pure Eu(II) in the investigated EuRhIn sample. At 78 K the spectrum shows a single signal at $\delta = -8.30(2)$ mm/s, subjected to quadrupole splitting of 10(1) mm/s. In our previous investigations on the series EuTIn (T = Zn, Pd, Pt, Au), we could show that the largely varying isomer shifts were linearly correlated with the shortest Eu–Eu distances (8). EuRhIn also fits well in this series, however, with the shortest Eu–Eu distance and the smallest isomer shift (Fig. 6).

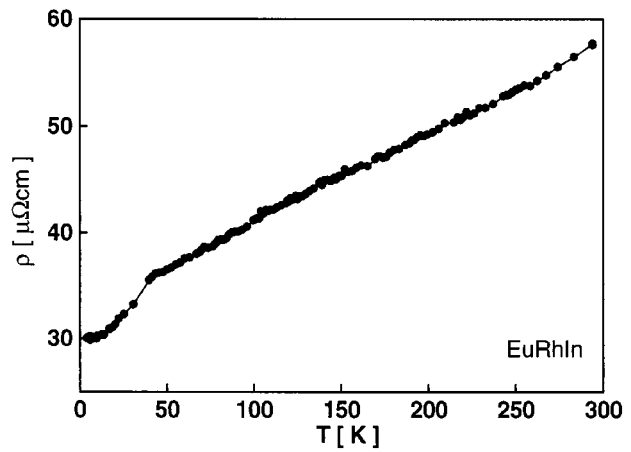

FIG. 4. Temperature dependence of the specific resistivity of EuRhIn.

The onset of magnetic ordering in EuRhIn is already detected at 30 K (see Table 5) in the ^{151}Eu Mössbauer spectroscopic experiments, slightly higher than the Curie temperature of 22.0(5) K determined from the susceptibility data. The static magnetic flux density at the europium nucleus, however, is only 1.7(9) T at 30 K. Full magnetic hyperfine field splitting is observed at 4.2 K (Fig. 5) with a static magnetic flux density of 22.6(2), as frequently observed in such equiatomic intermetallic compounds (6, 8, 21). The temperature dependence of the internal magnetic hyperfine field at the europium nucleus approximately follows the Brillouin function for $J = 7/2$ (Fig. 6).

Crystal Chemistry

EuRhIn, the first compound in the ternary system europium–rhodium–indium, adopts the TiNiSi type structure (22). The latter represents a ternary ordered version of the KHg_2 type (23). In EuRhIn the rhodium and indium atoms are ordered on the mercury site. The structure of EuRhIn is presented in Fig. 7. It consists of strongly puckered Rh_3In_3 hexagons with Rh–In distances ranging from 277 to 279 pm. These are only slightly larger than the sum of Pauling's single bond radii, 275 pm for rhodium and indium (24). Stronger Rh–In bonding (264–275 pm) is observed in binary $RhIn_3$ (25). Because of the strong distortions of the hexagons, each indium atom has a distorted tetrahedral environment of the rhodium atoms, and vice versa. The europium atoms occupy the large cavities within the three-dimensional [RhIn] polyanion. The europium atoms are by far the most electropositive component of EuRhIn, and they will largely have transferred both valence electrons to the [RhIn] polyanion as is proved from the susceptibility and ^{151}Eu Mössbauer spectroscopic data. Considering the

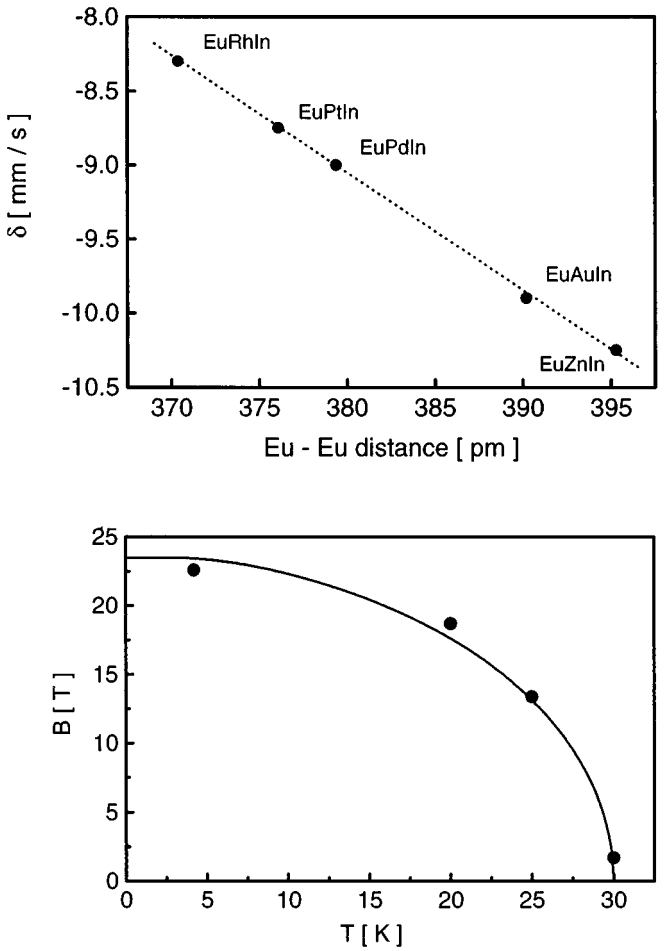

FIG. 6. Correlation between the shortest Eu–Eu distance and the isomer shift δ at 78 K for EuRhIn, EuZnIn, EuPdIn, EuPtIn, and EuAuIn (upper part). In the lower drawing the temperature dependence of the internal magnetic hyperfine field at the europium nucleus in EuRhIn is shown. It approximately follows the Brillouin function for $J = 7/2$.

almost covalent Rh–In bonding within this polyanion, the formula of our compound can to a first approximation be written as $Eu^{2+}[RhIn]^{2-}$.

Among the series of equiatomic Eu*T*In and Eu*T*Sn compounds, EuRhIn is the compound with the lowest electron count. In agreement with the trend of the tilts of the parallelograms between the distorted hexagonal network, we observe a Rh–In–Rh angle of 108.4°, comparable with the In–Pd–In angle of 109.8° in isotypic CaPdIn (26). A more detailed description of the crystal chemistry of such europium intermetallics within the TiNiSi family of compounds and of other ordering variants was given recently in references 4 and 27. Chemical bonding in the KHg_2 structure and its ternary derivatives was recently studied in detail by Nuspl *et al.* (26).

The $MgCu_2$ type Laves phase $EuIr_2$ has so far only been reported from X-ray powder data (11). These investigations

TABLE 5
^{151}Eu Mössbauer Fitting Parameters for EuRhIn as a Function of Temperature

T (K)	Γ (mms^{-1})	δ (mms^{-1})	ΔE_Q (mms^{-1})	B (T)
300	2.3(3)	− 8.36(8)	10(1)	–
78	2.3(1)	− 8.30(2)	10(1)	–
35	2.4(5)	− 8.2(1)	10(2)	–
30	2.4(4)	− 8.2(1)	10	1.7(9)
25	2.4(4)	− 7.8(2)	10	13.5(4)
20	2.3	− 7.8(1)	9(1)	18.7(2)
4.2	2.4	− 7.9(1)	8(1)	22.6(2)

Note. The numbers in parentheses give the statistical errors in the last digit. Values without parentheses were kept fixed by the fitting program.
δ, isomer shift with respect to EuF_3; Γ, experimental line width; ΔE_Q, electric quadrupole interaction; B, static magnetic flux density.

are fully confirmed by our single crystal data. A separate refinement of the occupancy parameters gave no indication for a deviation from the correct composition. The iridium atoms build a three-dimensional network of corner-sharing tetrahedra with Ir–Ir distances of 268 pm, slightly shorter than the Ir–Ir distances of 272 pm in fcc iridium (28). A cutout of the $EuIr_2$ structure is presented in Fig. 8. Each europium atom in $EuIr_2$ has 12 iridium neighbors at 314 pm and 4 europium neighbors at 328 pm. Together, the europium and iridium atoms form a Frank–Kaspar polyhedron

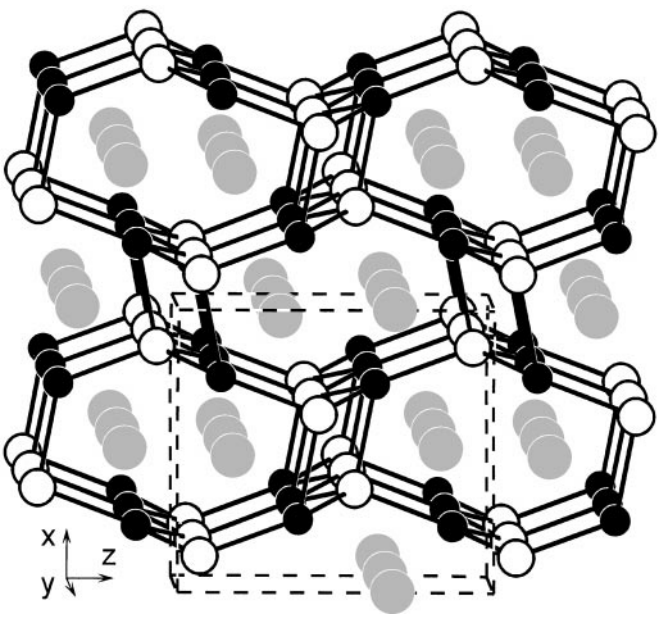

FIG. 7. View of the crystal structure of EuRhIn approximately along the *y* axis. The europium, rhodium, and indium atoms are drawn as gray, black, and open circles, respectively. The three-dimensional [RhIn] polyanion is emphasized.

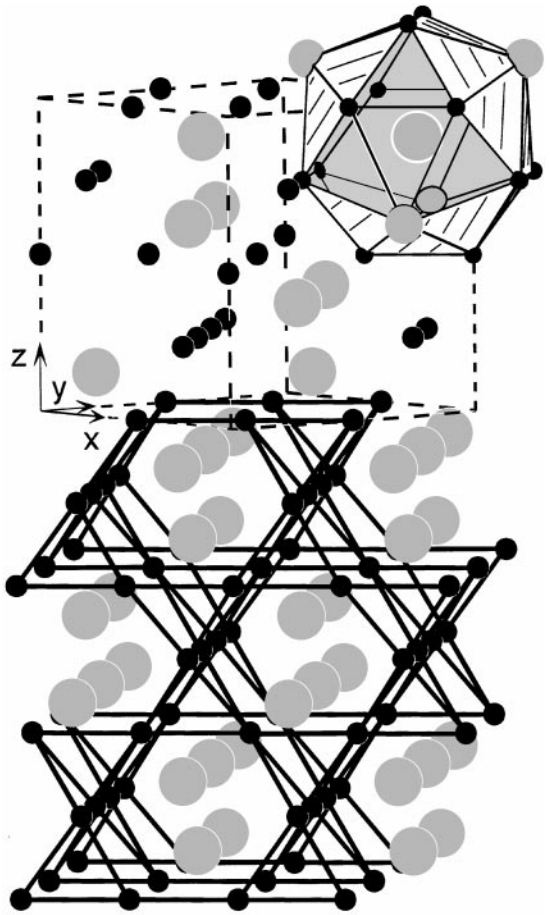

FIG. 8. Crystal structure of the cubic Laves phase $EuIr_2$. Emphasized are the unit cell, including one CN16 Frank–Kasper polyhedron, and the three-dimensional network of condensed Ir_4 tetrahedra.

(29, 30) of coordination number (CN) 16 around each europium atom. $EuIr_2$ has 20 valence electrons per formula unit. In good agreement with the structure–bonding relationships recently investigated by Johnston and Hoffmann (31) by extended Hückel band structure calculations, the cubic form of the Laves phase is stable for $EuIr_2$. The divalent character of the europium atoms in $EuIr_2$ was determined from magnetization measurements by Bozorth *et al.* (32).

The new stannide $EuIrSn_2$ crystallizes with the $MgCuAl_2$ structure (33), a ternary ordered version of the Re_3B type (34). With respect to the Re_3B structure, the europium and tin atoms are ordered on the rhenium sites. From a commonly used geometrical point of view, the europium and tin atoms build trigonal prisms of composition $[Eu_2Sn_4]$ that are centered by the iridium atoms as outlined in Fig. 9. These trigonal prisms are condensed via common faces forming one-dimensional rows. Neighboring rows are shifted with respect to each other by one-half of the *a* axis.

A closer look at this structure, however, reveals an interesting relationship with the structure of the Zintl phase $CaIn_2$ (35). The tin atoms in $EuIrSn_2$ build strongly puckered, elongated hexagons as outlined in the lower part of Fig. 9. The layers of these hexagons have the stacking sequence ABAB. The Sn–Sn distances within the hexagons of 322 pm ($4\times$) and 343 pm ($2\times$) are somewhat longer than between the hexagons (303 pm). These Sn–Sn distances compare well with those in β-tin, where each tin atom has fou Wr neighbors at 302 pm and two further neighbors at 318 pm (28). The tin network in $EuIrSn_2$ is actually a slight distortion of the lonsdaleite net (i.e., "hexagonal diamond"), modified by additional Sn–Sn bonds parallel to the *x* axis (28). Because of the elongation of the tin hexagons, the cavities in the polyanion are large enough to be occupied by the europium and iridium atoms. The latter have strong interactions with the tin polyanion. Each iridium atom has six tin neighbors at an average Ir–Sn distance of 274 pm, slightly longer than the sum of Paulings single bond radii of 266 for iridium and tin (24). Similar Ir-Sn distances (271 to

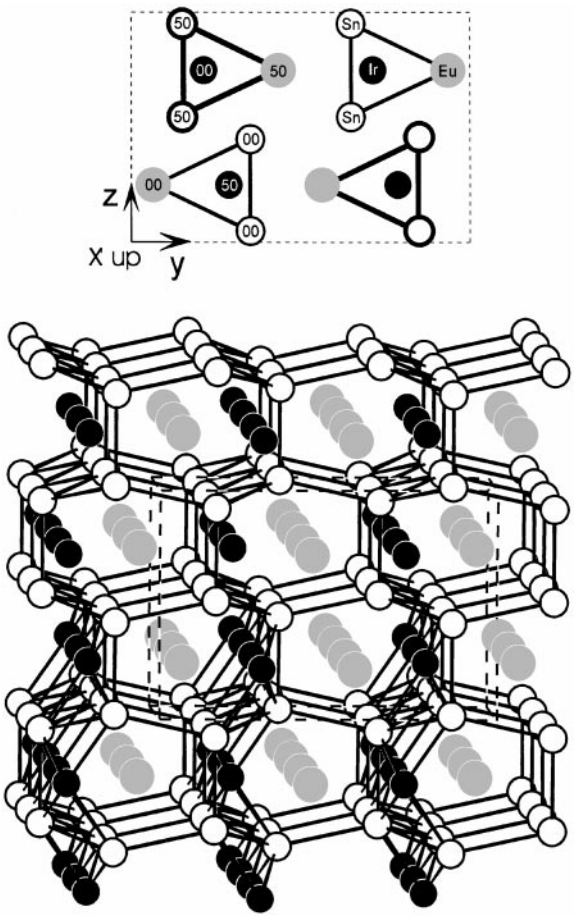

FIG. 9. Crystal structure of $EuIrSn_2$. A projection is shown in the upper drawing with an emphasis on the platinum centered trigonal $[Eu_2Sn_4]$ prisms. The three-dimensional polyanionic $[IrSn_2]$ network is outlined below. For clarity, only Sn–Sn bonds are shown in the upper part of this drawing.

287 pm) also occur for the eight tin neighbors of the iridium atoms in α-$IrSn_4$ (36). The Ir-Sn polyanion is emphasized in the lower part of Fig. 9. Although no magnetic data are available for $EuIrSn_2$, we assume that the europium atoms are most likely divalent and have transferred their two valence electrons to the polyanion. We can then to a first approximation assume a formulation $Eu^{2+}[IrSn_2]^{2-}$.

The $MgCuAl_2$ type structure has up to now been identified for more than 30 intermetallic phases (37). Very recently we discovered a couple of new isotypic compounds with calcium, strontium, europium, and ytterbium as the electropositive component (38–40). For a more detailed description of chemical bonding in such compounds based on extended Hückel and LMTO calculations, we refer to references 38 and 40.

ACKNOWLEDGMENTS

We thank Professor Wolfgang Jeitschko and Professor Hellmut Eckert for their interest in and support of this work. We are also indebted to Klaus Wagner for the EDX analyses and to Dr. Wolfgang Gerhartz (Degussa AG) for generous gifts of rhodium and iridium powder. This work was financially supported by the Deutsche Forschungsgemeinschaft (Po573/1-2) and the Fonds der Chemischen Industrie.

REFERENCES

1. C. Tomuschat and H.-U. Schuster, *Z. Anorg. Allg. Chem.* **518,** 161 (1984).
2. J. Evers, G. Oehlinger, K. Polborn, and B. Sendlinger, *J. Solid State Chem.* **91,** 250 (1991).
3. G. Michels, C. Huhnt, W. Scharbrodt, W. Schlabitz, E. Holland-Moritz, M. M. Abd-Elmeguid, H. Micklitz, D. Johrendt, V. Keimes, and A. Mewis, *Z. Phys. B* **98,** 75 (1995).
4. R. Pöttgen, *Z. Kristallogr.* **211,** 884 (1996).
5. F. Merlo, M. Pani, and M. L. Fornasini, *J. Alloys Compd.* **232,** 289 (1996).
6. R. Pöttgen, R.-D. Hoffmann, R. Müllmann, B. D. Mosel, and G. Kotzyba, *Chem. Eur. J.* **3,** 1852 (1997).
7. C. Felser, S. Cramm, D. Johrendt, A. Mewis, O. Jepsen, G. Hohlneicher, W. Eberhardt, and O. K. Andersen, *Europhys. Lett.* **40,** 85 (1997).
8. R. Müllmann, B. D. Mosel, H. Eckert, G. Kotzyba, and R. Pöttgen, *J. Solid State Chem.* **137,** 174 (1998).
9. Yu. Grin, R. Pöttgen, and R.-D. Hoffmann, *Z. Kristallogr.* **16** (suppl.), 55 (1999).
10. C. Lux, A. Mewis, S. Junk, A. Gruetz, and G. Michels, *J. Alloys Compd.* **200,** 135 (1993).
11. R. P. Elliott, "Proceedings of the Conference of Rare Earth Research, 4th, Phoenix, Arizona," p. 215 (1965).
12. H. L. Krauss, and H. Stach, *Z. Anorg. Allg. Chem.* **34,** 366 (1966).
13. R. Pöttgen, A. Lang, R.-D. Hoffmann, B. Künnen, G. Kotzyba, R. Müllmann, B. D. Mosel, and C. Rosenhahn, *Z. Kristallogr.* **214,** 143 (1999).
14. R.-D. Hoffmann, R. Pöttgen, unpublished results.
15. K. Yvon, W. Jeitschko, and E. Parthé, *J. Appl. Crystallogr.* **10,** 73 (1977).
16. G. M. Sheldrick, "SHELX-86, Program for the Solution of Crystal Structures," University of Göttingen, Germany, 1986.
17. G. M. Sheldrick, "SHELXL-97, Program for Crystal Structure Refinement," University of Göttingen, Germany, 1997.
18. A. Szytuła and J. Leciejewicz, "Handbook of Crystal Structures and Magnetic Properties of Rare Earth Intermetallics." CRC Press, Boca Raton, FL, 1994.
19. R. Pöttgen, *J. Mater. Chem.* **6,** 63 (1996).
20. T. Ito, S. Nishigori, I. Hiromitsu, and M. Kurisu, *J. Magn. Magn. Mater.* **177–181,** 1079 (1998).
21. U. Ernet, R. Müllmann, B. D. Mosel, H. Eckert, R. Pöttgen, and G. Kotzyba, *J. Mater. Chem.* **7,** 255 (1997).
22. C. B. Shoemaker and D. P. Shoemaker, *Acta Crystallogr.* **18,** 900 (1965).
23. E. J. Duwell and N. C. Baenziger, *Acta Crystallogr.* **8,** 705 (1955).
24. L. Pauling, "The Nature of the Chemical Bond and The Structures of Molecules and Crystals." Cornell University Press, Ithaca, NY, 1960.
25. R. Pöttgen, R.-D. Hoffmann, and G. Kotzyba, *Z. Anorg. Allg. Chem.* **624,** 244 (1998).
26. G. Nuspl, K. Polborn, J. Evers, G. A. Landrum, R. Hoffmann, *Inorg. Chem.* **35,** 6922 (1996).
27. D. Kußmann, R.-D. Hoffmann, and R. Pöttgen, *Z. Anorg. Allg. Chem.* **624,** 1727 (1998).
28. J. Donohue, "The Structures of the Elements." Wiley, New York, 1974.
29. F. C. Frank and J. S. Kaspar, *Acta Crystallogr.* **11,** 184 (1958).
30. F. C. Frank and J. S. Kaspar, *Acta Crystallogr.* **12,** 483 (1959).
31. R. L. Johnston and R. Hoffmann, *Z. Anorg. Allg. Chem.* **616,** 105 (1992).
32. R. M. Bozorth, B. T. Matthias, H. Suhl, E. Corenzwit, and D. D. Davis, *Phys. Rev.* **115,** 1595 (1959).
33. H. Perlitz and A. Westgren, *Ark. Kemi, Mineral. Geol.* **16B,** 1 (1943).
34. B. Aronsson, M. Bäckman, and S. Rundqvist, *Acta Chem. Scand.* **14,** 1001 (1960).
35. A. Iandelli, *Z. Anorg. Allg. Chem.* **330,** 221 (1964).
36. A. Lang and W. Jeitschko, *J. Mater. Chem.* **6**, 1897 (1996).
37. P. Villars and L. D. Calvert, "Pearson's Handbook of Crystallographic Data for Intermetallic Phases," 2nd ed. American Society for Metals, Materials Park, OH, 1991, and desk edition, 1997.
38. R.-D. Hoffmann, R. Pöttgen, G. A. Landrum, R. Dronskowski, B. Künnen, and G. Kotzyba, *Z. Anorg. Allg. Chem.*, in press.
39. Ya. V. Galadzhun, R.-D. Hoffmann, G. Kotzyba, B. Künnen, B. D. Mosel, R. Müllmann, and R. Pöttgen, *Eur. J. Inorg. Chem.*, in press.
40. R.-D. Hoffmann, U. Ch. Rodewald, and R. Pöttgen, *Z. Naturforsch. B* **54,** 38 (1999).